[5]For a discussion of bound-exciton complexes see, for example, J. J. Hopfield, in *Proceedings of the Seventh International Conference on the Physics of Semiconductors, Paris*, 1964 (Dunod, Paris, 1964), p. 725.

[6]E. J. Johnson, I. Filinski, and H. Y. Fan, in *Proceedings of the International Conference on the Physics of Semiconductors, Exeter*, 1962 (The Institute of Physics and the Physical Society, London, 1962), p. 375; E. J. Johnson and H. Y. Fan, Phys. Rev. 139, A1991 (1965).

[7]E. J. Johnson, in *Semiconductors and Semimetals*, edited by R. K. Willardson and A. C. Beer (Academic, New York, 1967), Vol. 3, p. 153.

[8]F. H. Pollak and M. Cardona, Phys. Rev. 172, 816 (1968); in the second of Eqs. (13), the coefficient in front of the term "$(\delta E_{001}+3\delta E_{111})^2/\Delta_0$" should read $-\frac{1}{32}$ instead of $-\frac{1}{4}$.

[9]R. L. Agarwal and M. Reine, Bull. Am. Phys. Soc. 14, 736 (1969).

[10]H. Hasegawa, Phys. Rev. 129, 1029 (1963).

[11]M. Reine, R. L. Aggarwal, and B. Lax, Solid State Commun. 8, 35 (1970).

[12]K. Suzuki and J. C. Hensel, Bull. Am. Phys. Soc. 14, 113 (1969).

[13]For the values of the S_{ij} used in this work see H. B. Huntington, in *Solid State Physics*, edited by F. Seitz and D. Turnbull (Academic, New York, 1958), Vol. 7.

[14]I. Balslev, Phys. Rev. 143, 636 (1966).

[15]L. D. Laude, F. H. Pollak, and M. Cardona, Phys. Rev. B (to be published).

[16]P. Lawaetz, Phys. Rev. B (to be published).

[17]B. J. Roman and A. W. Ewald, Bull. Am. Phys. Soc. 13, 408 (1968); and private communication.

[18]D. W. Langer, R. N. Euwema, K. Era, and T. Koda, Phys. Rev. B (to be published).

[19]M. A. Gilleo, P. T. Bailey, and D. E. Hill, J. Luminescence 1/2, 562 (1970).

[20]R. R. Sharma and S. Rodriguez, Phys. Rev. 153, 823 (1967); 159, 649 (1967).

[21]P. T. Bailey, Phys. Rev. B 1, 588 (1970).

Study of the Shape of Cyclotron-Resonance Lines in Indium Antimonide Using a Far-Infrared Laser

J. R. Apel* and T. O. Poehler

Applied Physics Laboratory, The Johns Hopkins University, Silver Spring, Maryland 20910

and

C. R. Westgate and R. I. Joseph

The Johns Hopkins University, Baltimore, Maryland 21218

(Received 18 May 1970)

An experimental and theoretical study of the shape of cyclotron-resonance lines in high-purity n-type InSb has been conducted at cryogenic temperatures, using a repetitively pulsed far-infrared gas laser at $\lambda = 336.8$, 118.6, 78.4, 55.1, and 47.5 μm. Measurements of the 4.2 °K effective mass and scattering times have been obtained as a function of frequency via transmission through a thin sample arranged in the Faraday configuration. For carriers at a concentration of 1×10^{14} cm^{-3}, one obtains a zero-field 4.2 °K effective-mass ratio of 0.0139 ±0.0002. At laser frequencies below the optical-phonon frequencies, an anomalous narrowing of the lines was observed whose width implies a collision time τ near 10^{-11} sec, which is about 160 times longer than the value derived from dc magnetoconductivity at 20 kG. The theoretical analysis uses the quantum plasma dielectric tensor $\overleftrightarrow{\epsilon}(\vec{q}, \omega)$ complete with a collisional energy term of the form $\Delta + i\Gamma$ and a nonparabolic energy expression for conduction-band electrons. The dispersion equations for photon propagation in the Faraday and Voigt geometries are then solved to obtain the cyclotron-resonance line shape, using both constant- and energy-dependent collision times. It is shown that the observed line shapes and widths may be predicted without adjustable parameters to within the experimental error by a scattering time $\tau(\vec{B}, k_s)$, which describes adiabatic and nonadiabatic Coulomb scattering. Thus the narrowed lines are attributed to the reduced scattering rate from long-range ionized impurities that occurs in the quantum limit $\hbar\omega_c > k_B T$. Another experiment, done in the Voigt configuration at 77 °K using $\lambda = 336.8$ μm, yielded at 4.5-kG mass ratio of 0.0132 ±0.0002 and a scattering time of 2.75×10^{-12} sec, which is within a factor of 2 of the zero-field mobility time.

I. ON INTENT AND EXTENT

There is much information on the nature of carrier states to be obtained from a detailed examination of the shape of a cyclotron-resonance curve. In principle, a single precise measure of cyclotron resonance that is used in conjunction with a suitable theory would allow one to deduce the numerical

values of carrier effective mass, scattering time, electron temperature, static conductivity, and concentration. A series of such measurements taken versus wavelength, magnetic field, or temperature can be made to yield functional forms for these quantities. Finally there are impurities, polarons, hot-electron effects, and combined spin and cyclotron resonances which may be plumbed by the techniques.

In order to carry out resonance experiments in materials having scattering times $\tau \approx 10^{-13}$ sec, the obvious route to follow is toward far-infrared frequencies, since one requirement for a well-defined resonance, $\omega_c \tau \gg 1$, cannot nominally be met at centimeter wavelengths in a crystal having a scattering time of that order. Nevertheless, Dresselhaus and co-workers[1] managed to obtain an effective-mass measurement of $m = 0.013 m_0$ in InSb at 24 GHz by lowering the temperature to $1.2 °K$, whereupon a resonance appeared.

Until the appearance of the far-infrared gas laser,[2,3] the experimenter was forced to rely upon filtered thermal sources for his signal probe of cyclotron resonance. Several of the earlier experiments[4-6] served to delineate some of the problems in InSb, of which the ones of sensitive detectors and broad-band sources appeared especially severe. As far-infrared techniques improved, however, experimentation in this region of the spectrum became easier. By using pulsed fields as large as 330 kG and pass-band filtered thermal sources with wavelengths as short as 9.4 μm, Lax et al.[7] mapped out the variation of the room-temperature effective mass in InSb at magnetic fields above 90 kG. Within two weeks of the appearance of the paper reporting these results, Palik and collaborators published a complementary but somewhat overlapping study extending down to 25 °K in temperature and 10 kG in field.[8] Most recently, Johnson and Dickey have completed a comprehensive study of InSb cyclotron resonance and the interaction of resonant electrons with other excitations in the solid, again at cryogenic temperatures.[9]

While these experiments were eminently successful in terms of effective-mass measurements and electron-lattice interplay, the low power of the thermal sources and the necessarily wide-band radiation ($\Delta\lambda/\lambda$ of the order of 1–25%) did not allow the detailed studies of resonance line shapes that the monochromatic microwave sources had.

The far-infrared laser immediately resolved the low-power and the broad-band problems, but these devices required one to operate at a small finite number of infrared wavelengths. Button et al.[10] chose $\lambda = 337$ μm from a pulsed HCN laser as a probe of Ge. Later Button and others[11] experimented with p-type InSb using the strong line at

$\lambda = 118.6$ μm from H_2O vapor in a study of the valence bands of that material. Apel and co-workers[12] demonstrated cyclotron quantum effects in n-type InSb at $4.2 °K$, again using the line at 118.6 μm. Several of these investigations showed discrete structure in the lines,[8,9,12] illustrating the need for a quantum-mechanical treatment of cyclotron resonance.

How does one extract the information hidden in the shape of a cyclotron-resonance line? The answer lies in the proper theory. The simplest single-particle classical Drude theory gives for the left and right (lower and upper signs, respectively) polarized components of the conductivity

$$\text{Re}\,[\sigma_{\pm}(\omega)] = \sigma_0/[1 + (\omega \mp \omega_c)^2 \tau^2]\,, \tag{1}$$

where $\sigma_0 = n_c e^2 \tau/m$ is the static or dc conductivity due to electrons of concentration n_c and effective mass m, which surrender momentum through collisions at an average interval τ. We define ω_c to be the effective cyclotron frequency $|e|B/mc$ in a magnetic field B. Thus one measures only values for the effective mass, the scattering or relaxation time τ, and perhaps the conductivity, by applying Eq. (1) to an experiment.

But we know much more of the physics of the situation. There exists a whole series of calculations of the band structure of InSb, both in and out of a magnetic field, and the theoretical formulation should reflect these. In addition, a proper description of infrared (IR) photon propagation necessitates quantum kinetic theory, which in turn involves density matrices or master equations or other esoterica. One result of this work is to demonstrate that it has been worth the trouble to use quantum transport theory, and the next several pages are an exposition of its application to cyclotron resonance.

II. SURVEY OF EXPERIMENT

The experiment in general has addressed itself to electron cyclotron resonance in high-purity InSb at far-infrared wavelengths ranging from 337 to 48 μm, with the crystal held at temperatures of either 4.2 or 77 °K. Its intent was to exploit the spectral purity and comfortable power levels of a far-infrared gas laser in studying the detailed shape of the resonance line. In particular, the nature of the scattering mechanisms at low temperatures was of interest, since in the quantum limit, where $\hbar\omega_c \gg k_B T$, ionized impurity scattering in the presence of a magnetic field may be examined without the interference of phonons. The experiment dealt in transmission measurements, since these are the simplest to implement and there are no perturbing leads or contacts on the sample.

A 66-kG 2.5-cm-bore 15-cm-long superconducting magnet was available for use in experiments at liquid-He temperature; it was convenient for op-

erating in the Faraday geometry, where the photon wave vector $\vec{q}$ is parallel to the static magnetic field $\vec{B}$. In addition, a small electromagnet, limited to 14 kG with a liquid-N_2 Dewar, was used for experiments in the Voigt geometry ($\vec{q}$ normal to $\vec{B}$). In the latter configuration, data were taken with polarization of the laser photon field $\vec{E}$ either perpendicular or parallel to the magnetic field.

All of the transmission data were obtained from a high-purity sample of n-type InSb, of approximate volume $\Omega = 6 \times 8 \times 0.08$ mm^3, cut normal to the [111] axis and etched in the acid etch CP-4 to the desired thickness. Its 77 °K concentration was 1×10^{14} cm^{-3} and its dc mobility $\mu_0 = 6.7 \times 10^5$ cm^2/V sec. It was glued to a high-resistance Ge substrate using cellulose tridecanoate, a cement that remains plastic at helium temperatures, thus avoiding sample strain. In the Faraday geometry, the wafer was mounted in an aperture in the 1.27-cm-i.d. stainless-steel pipe which served as an IR transmission device, and was centered in the bore of the superconducting magnet. In the Voigt geometry, a similar aperture held sample and substrate between optical windows in the Dewar tail.

Figure 1 is a simplified schematic drawing of the Faraday arrangement.

The long-wavelength IR detector was an InSb crystal having $n_c = 2 \times 10^{13}$ cm^{-3}, $\mu_0 = 3 \times 10^5$ cm^2/V sec at 77 °K, and $\Omega = 1.5 \times 1.5 \times 10$ mm^3. Current leads were soldered to the small ends with In solder, and the photoconductive signal was observed by the change in voltage across the sample when biased at 50 μA from a constant current source. It was mounted in a triple magnetic shield about 10 cm below the solenoid, as shown on Fig. 1. The device served as a fast square-law sensor of the free-electron bolometer variety[13] for those transmitted signals having wavelengths ranging from several mm to 150 μm, and yielded about 100 μV/μW for power levels below about 10 mW.
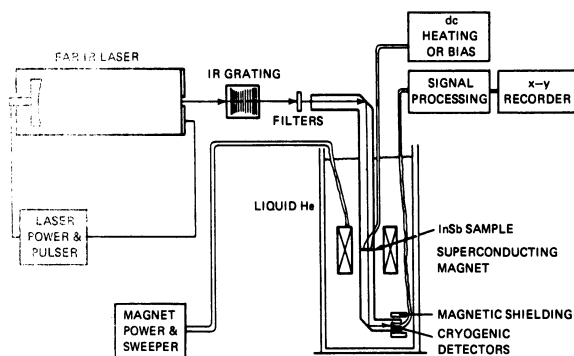
The other shielded detector was a Ga-doped Ge

photodetector of similar size and sensitivity, working between approximately 30 and 120 μm.

The gas laser, which has been described in detail in other publications,[12,14-16] was a 6-m-long 15-cm-diam device of semiconfocal optical configuration which was pulsed at 19 pulses/sec with a 4–6 kV several-thousand-ampere capacitor discharge. A wide range of wavelengths was available, including the water vapor lines with wavelengths $\lambda = 118.6$, 78.4, 55.1, and 47.5 μm; in HCN (obtained from an N_2-CH_4 mixture), the 336.8-μm line was used. These lines were filtered with IR gratings, quartz, and polyethylene as required, to ensure monochromaticity.

While several watts of IR power were available at higher-power inputs, the requirements of steady signal, spectral filtering, and light-pipe transmission led to power levels incident on the sample between 10 and 100 μW. Higher levels were undesirable as a possible source of electron heating. We estimate that at a lattice temperature $T = 4.2$ °K, the 100-μW laser pulse resulted in an increment in electron temperature T_e of less than three degrees.

The IR detector output signals were processed in a train of electronics consisting of (a) preamplification, (b) gated integration, (c) synchronous phase-coherent detection, and (d) recording as a function of magnetic field. Because of the noise level from the high-power pulsed discharge in the laser, some care was required to isolate the low-level-signal circuits. When properly carried out, the limiting noise in the system came from amplitude fluctuations in the laser IR output. Under good conditions, this was several percent of the peak signal.

III. PROPERTIES OF InSb

A. Properties and Parameters

At 4.2 °K, a crystal with $n_c = 1 \times 10^{14}$ cm^{-3} has its chemical potential ζ lying in the conduction band, so that it is mildly metallic. Table I lists a number of parameters for the sample used; it also serves to define many of the quantities in the mathematical development to follow.

B. Band Structure

There have been several publications dealing with the band structure of InSb in a magnetic field.[7,17-22] Usually the results are given in the form of numerical solutions to high-order matrix equations and yield energies $\mathcal{E}_b(\vec{k})$ for the conduction band and the three valence bands under specific numerical assumptions. However, simplified analytic results have been given by Bowers and Yafet,[17,18] and while approximate, are highly useful and reasonably accurate expressions, and we will utilize them here.

FIG. 1. Schematic of cyclotron-resonance experiment as conducted in the Faraday configuration.

Since our attention is focused on electron cyclotron resonance in n-type material, we are interested in conduction-band levels only, which will be denoted by $\mathcal{E}(n, k_z, s)$. In terms of the band gap $\mathcal{E}_g$ and electron wave-vector component along the magnetic field direction k_z, the levels are given by

$$\mathcal{E}(n, k_z, s) = \tfrac{1}{2}\mathcal{E}_g \left\{ -1 \right.$$
$$\left. + \left[1 + \frac{4}{\mathcal{E}_g}\left(\frac{\hbar^2 k_z^2}{2m} + \hbar\omega_c(n + \tfrac{1}{2} \mp \tfrac{1}{2}\nu) \right) \right]^{1/2} \right\} .$$

$$(2)$$

Here $s = \mp$ gives the spin splitting, to be differentiated from the polarization convention $\pm$ used below. The parameter $\nu = gm/2m_0$ relates to the g factor. Using this equation, it is possible to match the published band-edge energy levels[20,21] in InSb for $0 \leq B \leq 25$ kG and $0 \leq n \leq 5$ to within approximately $\pm 2\%$, or to within the resolution of the graph, whichever is larger. In a recent paper, Johnson and Dickey[9] utilize a formula similar to Eq. (2) with small improvements that apparently extend its range of applicability to $B = 45$ kG. For $B \leq 25$ kG, such improvements lead to approximately 1% changes; thus Eq. (2) should be a good approximation for the present work.

Figure 2 is a graph of the first few levels of Eq. (2) at $B = 20$ kG for the region near the zone center; $\mathcal{E} = 0$ is the conduction-band edge. The nearly vertical transition $\Delta\mathcal{E}$ represents cyclotron-resonance absorption with initial quantum number $n = 0$ and $\Delta n = 1$, in accordance with a selection rule to be discussed. The small $\Delta k_z = q_z$ is supplied by the infrared photon.

An expansion of Eq. (2) for small values of its arguments gives

TABLE I. Properties and parameters for InSb at 4.2 °K.

| Quantity	Symbol	Value	Units
Electron concentration	n_c	1.0×10^{14}	cm^{-3}
Total impurity concentration	$N_d + N_a$	$\approx 10^{15}$	cm^{-3}
Effective mass	m	$0.0139m_0$	gm
Effective g factor	g	-50.3	...
dc mobility	μ_0	8.2×10^4	cm^2/V sec
dc momentum-scattering time	τ_0	6.8×10^{-13}	sec
Lattice dielectric constant	ϵ_l	16.5	...
Plasma frequency	ω_p	1.15×10^{12}	sec^{-1}
Chemical potential ($B = 0$)	ζ_0	$+0.15$	meV
Impurity ionization potential	$\mathcal{E}_i$	2.5 (20 kG)	meV
TO-phonon energy	$\hbar\omega_{t0}$	22.1	meV
LO-phonon energy	$\hbar\omega_{l0}$	24.2	meV
Quantum cyclotron radius	r_c	224 (20 kG)	10^{-8} cm
Debye shielding distance	$1/k_s$	575	10^{-8} cm
Mean distance between neutral impurities	$(N_d + N_a)^{-1/3}$	≈ 1000	10^{-8} cm
Reciprocal Fermi wave number	$1/k_F$	1250	10^{-8} cm
Mean distance between ionized impurities	$N_i^{-1/3}$	2150	10^{-8} cm
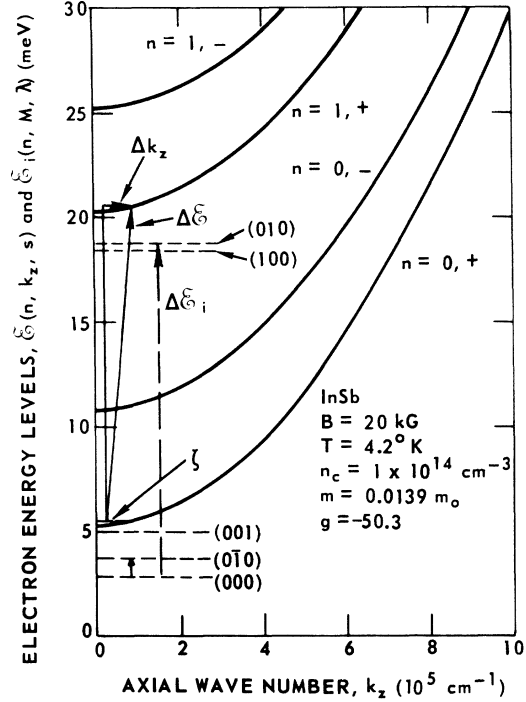
FIG. 2. InSb energy levels in a 20-kG magnetic field showing the first two spin-split Landau levels. The cyclotron-resonance transition is denoted by $\Delta\mathcal{E}$ and the most important impurity transition by $\Delta\mathcal{E}_i$.

$$\mathcal{E}(n, k_z, s) \simeq \frac{\hbar^2 k_z^2}{2m} + \hbar\omega_c(n + \tfrac{1}{2} \mp \tfrac{1}{2}\nu)$$
$$+ \left[\frac{1}{\mathcal{E}_g}\left(\frac{\hbar^2 k_z^2}{2m} + \hbar\omega_c(n + \tfrac{1}{2} \mp \tfrac{1}{2}\nu) \right)^2 \right] , \quad (3)$$

where the term in square brackets contributes about 2% to the ground-state energy at the band edge, in a 20-kG field. The first two terms are just the free-electron results,[23] but with the effective mass, cyclotron frequency, and g factor replacing the normal values. As is well known,[24] the effective-mass Hamiltonian H_0 corresponding to those terms is

$$H_0 = \frac{1}{2m}\left(-i\hbar\vec{\nabla} + \frac{eB}{c}\vec{x} \right)^2 + \hbar\omega_c\tfrac{1}{2}\nu\sigma_z , \quad (4)$$

and its eigenstates $|\alpha\rangle$, normalized to a large crystal volume $\Omega = L^3$, are

$$|\alpha\rangle = |nk_z k_y s\rangle = L^{-1} e^{i(k_y y + k_z z)}\Phi_n(x + k_y r_c^2)|\eta\rangle , \quad (5)$$

where the ket $|\eta\rangle$ is a spinor. Due to the choice of Landau gauge for the static magnetic field $\vec{B} = \vec{\nabla} \times \vec{A}_0$, i.e., $\vec{A}_0 = (0, xB, 0)$, the harmonic-oscillator functions Φ_n are displaced in the x direction by an amount $-k_y r_c^2$, the important parameter r_c being the expectation value of the ground-state cyclotron

radius,

$$r_c = (\hbar c/eB)^{1/2} \ . \tag{6}$$

Explicitly, the oscillator functions are

$$\Phi_n(x) = (2^n n!)^{-1}(m\omega_c/\pi)^{1/4}H_n(x/r_c)\,e^{-x^2/2r_c^2} \ ; \tag{7}$$

here H_n is a Hermite polynomial. Equation (5) is similar in form to the basis vectors used in the calculation leading to Eq. (2), but with the orbital states integrated out and their influence appearing instead in the effective mass and g factor.

The similarity of the eigenfunctions for free and effective-mass electrons means that much of the large body of literature dealing with the former is applicable to the latter. Where precise values for energies are required, or when nonparabolic effects are important in the degeneracy factor or the density of states, the more complete formula, Eq. (2), has been used; where simplified or noncritical results are allowed, the first two terms of Eq. (3) have sufficed. The chief effect of Eq. (2) is to replace the definition of the cyclotron frequency $\omega_c = eB/mc$ by the more complicated form

$$\omega_{n+1,n} = (1/\hbar)[\,\mathcal{E}(n+1,k_z,s) - \mathcal{E}(n,k_z,s)] \tag{8}$$

in certain sensitive equations.

C. Impurity Levels

At temperatures below 10–20 °K, the imposition of a magnetic field may freeze electrons to donor impurity sites in hydrogenlike states having an ionization potential $\mathcal{E}_i$ near 2 meV at 10 kG. These states have been studied by Kaplan[25] and Wallis and Bowlden[26] among others. Figure 2 also shows their approximate energy levels $\mathcal{E}_i(n,M,\lambda)$. The quantum numbers $(nM\lambda)$, respectively, denote the Landau number, the value of orbital angular momentum, and a variational parameter λ which goes over into k_z for electrons in the Landau continuum. The graph also illustrates a photon-induced impurity transition between the ground state $(n = M = 0)$ and one of higher orbital angular momentum $(n = 0, M = +1)$ lying below the $n = 1+$ continuum. The energy difference $\Delta\mathcal{E}_i = \mathcal{E}_i(0,1,0) - \mathcal{E}_i(0,0,0)$ is somewhat larger than the free-free cyclotron-resonance transition energy $\Delta\mathcal{E}$ and much larger than the ionization potential.

In an experiment, resonance lines with both $\Delta\mathcal{E}$ and $\Delta\mathcal{E}_i$ are observed, their amplitudes depending on the proportion of free to frozen carriers. Thus the importance of the impurity line depends on the temperature and the magnetic field strength.

IV. PLASMA DIELECTRIC TENSOR

In describing the free-carrier resonant absorption process, we choose to use the quantum formulation of the plasma dielectric tensor. Cyclotron resonance is then viewed as a special case of

electromagnetic wave propagation in an ionized magnetized dissipative medium. The dispersion equation which relates ω to $\vec{q}$ for photons behaving as $e^{i(\vec{q}\cdot\vec{r}-\omega t)}$ in such a medium is well known and methods of establishing the propagation characteristics have been highly developed.[27–29]

Some modification of the usual formulations are needed for the solid-state plasma at hand. In particular, collisions must be properly taken into account, which we have done by incorporating collision operators for ionized impurity scattering into the quantum transport equation. We have also approximated the lattice contribution to $\overleftrightarrow{\epsilon}$ with an isotropic function $\epsilon_l(\omega)$, taken to be constant at 16.5.

Reference 30 gives the development of the plasma dielectric tensor, generally modeled after Ron's[31] treatment for a degenerate free-electron gas. We have followed Kawabata[32] and Lodder and Fujita[33] by adding the collisional energy $U(\vec{r})$ directly into the equation of motion for the density operator ρ. This was done in preference to the relaxation-time approximation for collisional effects used by Greene[34] and predecessors because of the relative simplicity and elegance which result.

A. Equation of Motion

The one-electron density operator ρ in the Schrödinger picture evolves under the influence of the total Hamiltonian $H + U$ according to

$$i\hbar\,\frac{\partial\rho}{\partial t} + [H + U, \rho] = 0 \ . \tag{9}$$

The function H includes the static magnetic field $\vec{B} = \vec{\nabla}\times\vec{A}_0$ and the IR photon electric field

$$\vec{E}(\vec{r}, t) = \vec{E}(\vec{q}, \omega)e^{i(\vec{q}\cdot\vec{r}-\omega t)}$$

(treated semiclassically, for simplicity) in addition to the kinetic terms. Since spin transitions are not of interest, we neglect the electromagnetic $\vec{H}$ field.

In the usual fashion, one first linearizes Eq. (9) by expanding about a steady-state operator ρ_0, via $\rho(t) = \rho_0 + \rho_1(t)$. Here

$$\rho_0 = \sum_\alpha \ |\alpha\rangle f_0(\alpha)\langle\alpha| \ , \tag{10}$$

where $f_0(\alpha)$ is any steady-state distribution function. In all cases, we have used the Fermi distribution along with the InSb electron energy expression, Eq. (2). Thus

$$f_0(n, k_z, s) = \{e^{[\mathcal{E}(n,k_z,s)-\zeta]/k_B T} + 1\}^{-1} \ . \tag{11}$$

This choice implies care must be taken in the experiment neither to heat nor to redistribute the electrons. One also writes

$$H = H_0 + H_1 \ , \tag{12}$$

where H_0 is given by Eq. (4), and where H_1 incor-

porates the $\vec{E} \cdot (\vec{p} + e\vec{A}_0/c)$ term.

By applying a Kubo transport formula to the resultant equation, Kawabata[32] obtains a resonant denominator in $\tilde{\epsilon}$ of the form

$$[\hbar(\omega - \omega_c) + \Delta + i\Gamma]^{-1} ,$$

where $\Delta + i\Gamma$ are an energy shift and a broadening, respectively, due to electrons interacting with the scattering potential $U(\vec{r})$; we shall discuss these below. Exactly the same form is obtained if instead one substitutes for $[U, \rho]$ in Eq. (9) a term $(\Delta + i\Gamma)\rho_1$, which is a type of relaxation-time approximation, but with a complex energy replacing the usual $\hbar/\tau$. In either formulation, the linearized equation of motion becomes

$$\hbar\omega\rho_1 + [H_0, \rho_1] + [H_1, \rho_0] = (\Delta + i\Gamma)\rho_1 . \tag{13}$$

B. Dielectric Tensor

Using Eq. (13), one may compute the required current density by appropriate Fourier-Laplace transforms, a quantum-mechanical averaging, and

a thermal weighting of the current operator

$$\vec{J}_{op}(\vec{r}, t) = (- e/m)(\vec{p} + e\vec{A}/c) , \tag{14}$$

which must be written in symmetrized form and contain vector potentials for both $\vec{B}$ and $\vec{E}$. From such manipulations is obtained the observable $\vec{J}(\vec{q}, \omega)$:

$$\vec{J}(\vec{q}, \omega) = \frac{1}{\Omega} \operatorname{Tr}[(\rho_0 + \rho_1)\vec{J}_{op}(\vec{q}, \omega)]$$

$$= \overleftrightarrow{\sigma}(\vec{q}, \omega) \cdot \vec{E}(\vec{q}, \omega) . \tag{15}$$

The trace in Eq. (15) is composed of matrix elements taken between the $|\alpha\rangle$ states of Eq. (5). The second line defines the conductivity tensor $\overleftrightarrow{\sigma}(\vec{q}, \omega)$, which is related to the dielectric tensor $\overleftrightarrow{\epsilon}(\vec{q}, \omega)$ by

$$\overleftrightarrow{\epsilon}(\vec{q}, \omega) = \epsilon_l(\omega) \overleftrightarrow{1} + 4\pi i \overleftrightarrow{\sigma}(\vec{q}, \omega)/\omega . \tag{16}$$

The somewhat lengthy calculation found in Ron's paper[31] and Ref. 30 gives for that quantity

$$\overleftrightarrow{\epsilon}(\vec{q}, \omega) = \epsilon_l(\omega)\left\{\left(1 - \frac{\omega_p^2}{\omega^2}\right)\overleftrightarrow{1} - \frac{\omega_p^2}{\omega^2 \times 4\pi^2 n_c \hbar} \sum_{n,n',s} \int_{-\infty}^{\infty} dk_z \vec{F}_{n,n'}(\vec{q}, k_z)\vec{F}_{n,n'}^*(\vec{q}, k_z)\left[\frac{\omega_{n+1,n}\Delta f_0}{\Delta \mathcal{E} - \hbar\omega + i\Gamma}\right]\right\} , \tag{17}$$

where we have abbreviated by writing

$$\Delta f_0 = f_0(n', k_z + q_z, s) - f_0(n, k_z, s) , \tag{18}$$

$$\Delta \mathcal{E} = \mathcal{E}(n', k_z + q_z, s) - \mathcal{E}(n, k_z, s) + \Delta , \tag{19}$$

$$\omega_p^2 = 4\pi n_c e^2/\epsilon_l m , \tag{20}$$

and

$$\vec{F}_{n,n'}(\vec{q}, k_z) = \int_{-\infty}^{\infty} dx\, e^{iq_x x}\Phi_{n'}(x - q_y r_c^2)$$

$$\times [\hat{e}_x p_x - \hat{e}_y m\omega_c x + \hat{e}_z \hbar k_z - \tfrac{1}{2}\hbar\vec{q}]\Phi_n(x) . \tag{21}$$

The energy shift Δ is indistinguishable from the level difference in an experiment and thus has been incorporated into the definition of $\Delta\mathcal{E}$. Equation (20) defines the effective plasma frequency ω_p, and Eq. (21) the two-center integral[34,35] $\vec{F}_{n,n'}(\vec{q}, k_z)$. The sums in Eq. (17) are over initial and final Landau quantum numbers n and n', and over both spin states $s = \mp 1$; the k_z integral accounts for the wave-number distribution along the direction of the magnetic field and brings in thermal broadening and energy-dependent collision times. Since the solid must accommodate all of the carriers within its volume, the normalization is such that

$$n_c = \frac{1}{\Omega} \operatorname{Tr}(\rho_0) = \frac{m}{4\pi^2 \hbar} \sum_{n,s} \int_{-\infty}^{\infty} dk_z\, f_0(n, k_z, s)\omega_{n+1,n} . \tag{22}$$

An inversion of Eq. (22) gives the chemical potential ζ as a function of B, n_c, and T.

If the magnetic field is strong, or the transverse component of the photon wave vector small, so that $q_y r_c \ll 1$ (which is usually the case experimentally), the matrix form of $\tilde{\epsilon}$ reduces to

$$\overleftrightarrow{\epsilon}(\vec{q}, \omega) \simeq \begin{bmatrix} \epsilon_{xx} & -\epsilon_{xy} & 0 \\ \epsilon_{xy} & \epsilon_{xx} & 0 \\ 0 & 0 & \epsilon_{zz} \end{bmatrix} . \tag{23}$$

Thus there are three independent complex functions to evaluate. These functions take on their simplest form when the Faraday geometry is used [in which case Eq. (23) is exact]. For it the elements of interest are[36]

$$\epsilon_\pm = \epsilon_{xx} \pm i\epsilon_{xy} ,$$

the plus and minus signs corresponding to right and left circularly polarized waves, respectively,

propagating along the magnetic field, and should not be confused with the spin indices $\mp$. (We use the convention of plasma physics, with an electric vector having right polarization rotating in the same sense as do electrons in a magnetic field.) Equation (17) yields for this case

$$\frac{\epsilon_{\pm}}{\epsilon_{l}} = 1 - \frac{\omega_{p}^{2}}{\omega^{2}}\left(1 + \frac{m\omega_{c}}{4\pi^{2}\hbar n_{c}} \sum_{\substack{n=0 \\ s=\mp}}^{\infty} (n + \tfrac{1}{2} \pm \tfrac{1}{2})\right.$$

$$\left. \times \int_{-\infty}^{\infty} \frac{\Delta f_{0}\, dk_{z}\, \omega_{n+1,n}}{\omega_{n\pm1,n} - \omega + i/\tau}\right) , \qquad (24)$$

where $\tau = \hbar/\Gamma$; also $n' = n \pm 1$ only, as a result of the zero phase variation of the IR electric field across the diameter of a cyclotron orbit in this geometry.

C. Transmission and Absorption

From $\overleftrightarrow{\epsilon}(\vec{q}, \omega)$ one obtains the reflection, absorption, and transmission coefficients R, A, and T. In terms of the complex index of refraction $(n + i\kappa)$, the dispersion relations for the Faraday geometry $(\vec{q} \parallel \vec{B})$ are

$$(n_{\pm} + i\kappa_{\pm})^{2} = \epsilon_{\pm} . \qquad (25)$$

For the Voigt configuration $(\vec{q} \perp \vec{B})$, two cases also exist:

$$(n_{\perp} + i\kappa_{\perp})^{2} = 2\epsilon_{+}\epsilon_{-}/(\epsilon_{+} + \epsilon_{-}) \quad \text{for } \vec{E} \perp \vec{B} ,$$

while $\qquad\qquad\qquad\qquad\qquad\qquad\qquad (26)$

$$(n_{\parallel} + i\kappa_{\parallel})^{2} = \epsilon_{zz} \qquad \text{for } \vec{E} \parallel \vec{B} .$$

Explicitly separating real and imaginary components, one obtains the refractive index squared

$$n^{2} = \tfrac{1}{2}\{\text{Re}\epsilon + [(\text{Re}\epsilon)^{2} + (\text{Im}\epsilon)^{2}]^{1/2}\} , \qquad (27)$$

the absorption index

$$\kappa = (\text{Im}\epsilon)/2n , \qquad (28)$$

the absorption constant

$$\alpha = 2\omega\kappa/c , \qquad (29)$$

and the reflection coefficient

$$R = [(n-1)^{2} + \kappa^{2}]/[(n+1)^{2} + \kappa^{2}] , \qquad (30)$$

where the proper subscript $(+, -, \perp, \parallel)$ must be appended to each of these quantities, as the case requires.

Linearly polarized radiation is transmitted with $\vec{q} \parallel \vec{B}$ through a sample of thickness L according to

$$T_{F} = \tfrac{1}{2}[(1 - R_{+})e^{-\alpha_{+}L} + (1 - R_{-})e^{-\alpha_{-}L}], \qquad (31)$$

while the same quantity in the Voigt case is

$$T_{\perp,\parallel} = (1 - R_{\perp,\parallel})e^{-\alpha_{\perp,\parallel}L} . \qquad (32)$$

Thus, unless the sample thickness $L \ll 1/\alpha$, the transmission coefficient is not a linear function of $\text{Im}(\epsilon)$ or, equivalently, $\text{Re}(\sigma)$. From Eqs. (24) and

(29) one obtains

$$\alpha_{\pm} = \frac{4\pi}{n_{\pm}c} \frac{\omega_{c}}{\omega}\left(\frac{m}{4\pi^{2}\hbar n_{c}}\right) \sum_{n,s} (n + \tfrac{1}{2} \pm \tfrac{1}{2})$$

$$\times \int_{-\infty}^{\infty} dk_{z}\, \frac{\Delta f_{0}n_{c}e^{2}\tau(k_{z})\omega_{n+1,n}/m}{1 + (\omega_{n\pm1,n} - \omega)^{2}\tau^{2}(k_{z})} , \qquad (33)$$

where we have considered only the Faraday geometry. Even for the pure samples used, α_{+} ranged between 80 and 500 cm^{-1} at resonance. Thus, line distortion due to exponential absorption is nearly unavoidable in any reasonable thickness of these materials.

D. Scattering

At 4.2 °K, ionized impurity scattering governs the dc conductivity in InSb, while at 77 °K, phonons dominate; hence the dc mobility μ_{0} exhibits a maximum near 60–70 °K. One normally expects these mechanisms to continue to function at IR frequencies, since previous cyclotron-resonance experiments in other materials have yielded approximately the same scattering times at high microwave frequencies as those deduced from dc measurements.[37,38] Recently, however, experiments in GaAs[39] and CdTe[40] at 1- and 2-mm wavelengths have demonstrated anomalous narrowing of resonance lines as the temperature was lowered toward 10 °K. An analogous effect has been reported by us[41] for InSb; at 4.2 °K, the IR resonance lines became sharper as the magnetic field strengths and laser frequencies were increased. This is in direct contrast to the scattering time involved in dc magnetoresistance, which decreases as some inverse power of B at large field strengths.[24,42] The question then arises as to the correct form of τ to be used in Eq. (24).

1. Low Temperatures

Allowing ourselves to be guided by the soon-to-be-cited experimental results, we will discuss unshielded Coulomb scattering in the presence of a magnetic field and in the quantum limit, for this is apparently the governing mechanism in InSb at 4.2 °K. Such scattering is qualitatively different from zero-field impurity scattering, for which $\tau \sim \mathscr{E}^{3/2}$. The rationale for using an unshielded rather than a shielded Coulomb potential is that the collective effects responsible for the shielding cease to function effectively for electric fields oscillating above the plasma frequency ω_{p}.

Kawabata[32] has studied the theory of cyclotron-resonance linewidths using the Kubo technique for calculating the conductivity $\overleftrightarrow{\sigma}(\vec{q}, \omega)$ in the presence of losses. He derives the energy shift Δ and broadening $\Gamma = \hbar/\tau$ for a variety of scattering mechanisms in the quantum limit. The total scattering rate has

two contributions, termed nonadiabatic and adiabatic; Kawabata deals explicitly with only the former, while Kawamura[43] and Miyake[44] treat a special case of the latter. In the case of ionized impurities, nonadiabatic scattering arises when a collision between an electron and a scatterer causes the electron to redistribute its total energy among its internal states, these given by Eq. (2). In this transition, very little net energy is exchanged between light and heavy particles; the loss in forward momentum Δk_z appears as perpendicular momentum and hence energy. This loss must be great enough for the electron to achieve the adjacent Landau level or a transition is not allowed and only back scatter may occur. Thus, a Coulomb collision between an electron and a long-range ionized impurity induces the electron to barter part of its parallel energy $\hbar^2 k_z^2/2m$ for perpendicular energy $\hbar\omega_c(n+\frac{1}{2}\mp\frac{1}{2}\nu)$, or conversely. As the magnetic field increases, the adjacent Landau levels move farther apart and the electron must interact with increasingly larger Fourier components of the scattering potential in order to make a transition. Hence, the scattering time involves only the z component of momentum and lengthens with increasing B. Kawabata calculates a transport relaxation time $\tau_{\text{nonad}}(B)$ for the process which, for photon frequencies ω near ω_c, is

$$\tau_{\text{nonad}}(B) = \epsilon_i^2 \hbar \omega_c \left| \hbar k_z \right| / 2\pi N_i e^4 . \tag{34}$$

The time increases linearly with B and as $T^{1/2}$ for mildly degenerate electrons having $\hbar k_z \simeq (2mk_B T)^{1/2}$, and inversely as the concentration of ionized impurities N_i.

As B increases still further, the nonadiabatic process above becomes less and less likely. In the extreme quantum limit the scattering is instead dominated by an adiabatic broadening rate $1/\tau_{\text{ad}}(B)$ having the following physical origin: An electron with a small gyroradius r_c and impact parameter b senses the impurity force and its guiding center undergoes a drift motion at a velocity $\vec{v}_D = c\vec{E}_i \times \vec{B}/|\vec{B}|^2$ in the combined external magnetostatic field and impurity electrostatic field E_i. Thus, it drifts azimuthally with a frequency $\Omega_c \approx v_D/b$. This drift motion modulates the cyclotron frequency ω_c with a time variation that depends on the impact parameter, thereby introducing a spread of frequencies into the spectrum, but it does so without inducing nonadiabatic transitions as above. When appropriately averaged, the reciprocal of this frequency spread becomes $\tau_{\text{ad}}(B)$. Kawamura and co-workers[43] have obtained from the Coulomb potential and have verified the mass variation of the time

$$\tau_{\text{ad}}(B) = \left(\frac{15}{4\pi N_i}\right)^{1/2} \frac{\epsilon_i}{e^2} (m\hbar^2\omega_c)^{1/4} , \tag{35}$$

which behaves as $B^{1/4}$, a very weak dependence, and is independent of temperature.

Both processes described by Eqs. (34) and (35) occur simultaneously, of course, and the dominance of one or the other depends upon magnetic field strength and temperature.

2. Higher Temperatures

At liquid-N_2 temperatures, many Landau states are occupied and the conventional Boltzmann treatment of cyclotron-resonance scattering is probably quite sufficient. There appears to be little or no anomalous behavior in the 77 °K scattering times in GaAs,[39] CdTe,[40] Ge,[37] or p-type InSb,[38] nor do we observe any here, as will be discussed shortly.

V. CYCLOTRON-RESONANCE EXPERIMENTS

A. Conductivity Data in Faraday Configuration at 4.2°K

The five IR wavelengths mentioned previously were used to measure resonance line shapes in the high-mobility sample having $n_c = 1 \times 10^{14}$ cm^{-3}, as a function of magnetic field and laser frequency. Figure 3 shows the smoothed profiles for four of these five by way of the solid lines and theoretical fits to them (the dashed lines) to be discussed below.

Each line is seen to be a doublet; the low-field maximum is due to the impurity transition $\Delta\mathcal{E}_i$, and the high-field maximum is the free-electron cyclotron-resonance line. Since the sample is between two and four absorption lengths thick at resonance, the transmission coefficient does not represent the conductivity function but rather its exponentiated form. Therefore, the original data have been corrected to yield relative conductivities as derived from the logarithm of the transmission measurements. This technique assists immensely in decomposing a complex line into its underlying parts because doublet components may be added linearly, rather than logarithmically, to recover the envelope (cf. Fig. 3).

The impurity lines were analyzed using a simple Lorentz profile to determine resonant field B_i, half-width at half-maximum ΔB_i, and absolute conductivity.[26] These profiles are shown as the low-field components on Fig. 3. The free-electron resonance was then analyzed using the quantum calculation indicated by Eqs. (2), (22), (24), (25), and (27)–(31), with two separate functional forms taken for the scattering time τ; these will be discussed below. In general, it was possible to obtain an internally consistent fit to the width, amplitude, and integrated values of the impurity and free-electron lines only if magnetic freeze-out of the electrons on the donor sites was included in the calculation. The requirement that the total concentration of carriers, either free or frozen, must remain con-
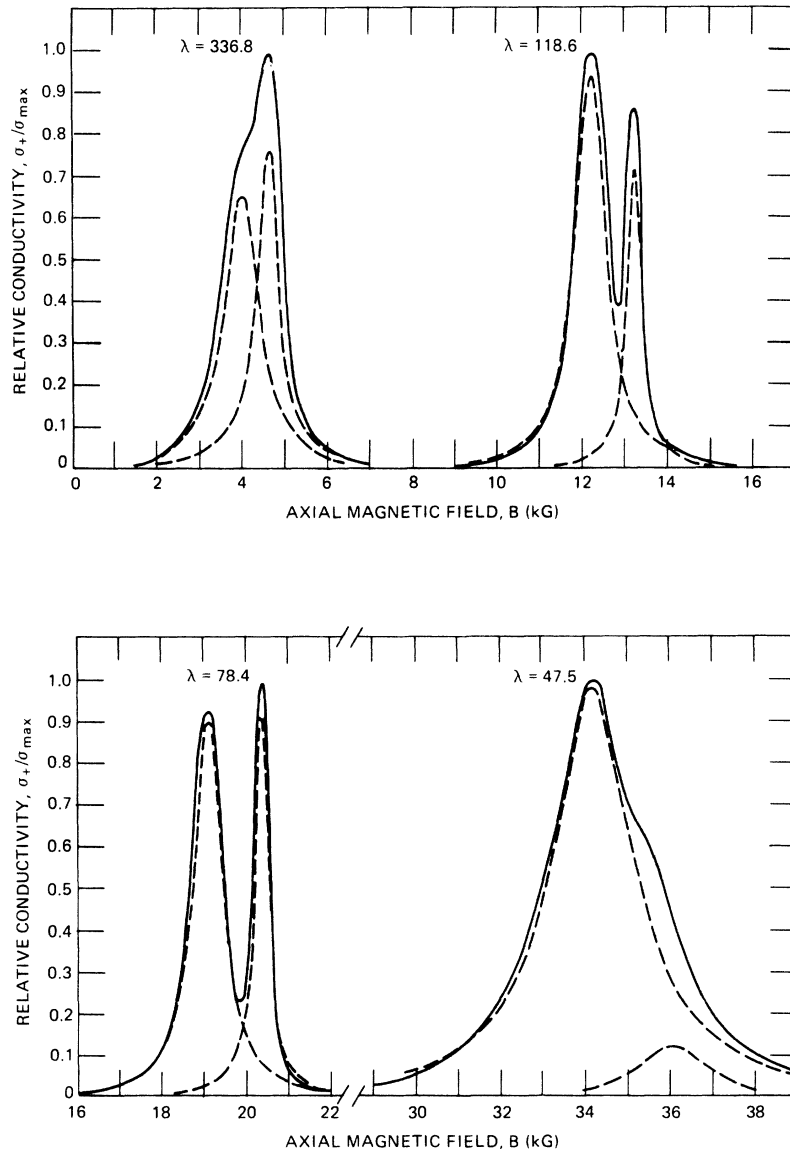
FIG. 3. Doublet lines from cyclotron resonance (the high-field peaks) and from impurity transitions (the low-field peaks), as observed in transmission at four laser wavelengths λ. Note the narrowing of the resonance lines as the wavelength increases from 336.8 to 78.4 μm, and the rebroadening above the optical-phonon field near 30 kG. The theoretical shapes of the three long-wavelength resonance lines are as predicted by Eqs. (24) and (36), using a field and momentum collision time $\tau(B, k_z)$; the impurity lines have been fitted with Lorentz profiles.

stant at 1×10^{14} cm^{-3} imposed another constraint that was useful in obtaining an unambiguous fit. The final calculated lines were required to acceptably match the data to within the experimental error as regards line position, half-width, maximum, and over-all shape.

While the underlying resonance lines at $\lambda = 336.8$ and 47.5 μm are not clearly separated, it is nevertheless possible to construct pairs of lines that reproduce these envelopes with reasonable fidelity; by utilizing the Lorentz profile to fit the low-field side of the impurity transition and the quantum profile for the high-field side of the cyclotron resonance, one may obtain line centers and widths to within less than 0.1 kG in both parameters.

B. Collision Times

Two approaches were taken to the determination of a collision time. The first assumed this quantity to be a constant, $\tau = \tau_c$, independent of B and k_z, to be used in Eqs. (24) and (27)–(31) and adjusted until theory and experiment agreed. Except for use of a quantum plasma tensor in place of the semiclassical Boltzmann description, this is the usual approach to deriving accurate values of τ from experimental data. The values for four laser lines obtained in this way are listed in Table II as τ_c and are also shown on Fig. 4 by the open circles for the three longest wavelengths. These scattering times are nearly an order of magnitude larger than the zero-field 4.2 °K dc time of $\tau_0 = 6.8 \times 10^{-13}$ sec.

TABLE II. Resonance parameters.

λ, μm	336.8	118.6	78.4	47.5
B_r (kG)	4.55	13.20	20.40	36.1
$(\alpha_+ L)_{max}$	2.70	3.22	2.92	3.12
τ_c (10^{-12} sec)	2.5	5.0	5.5	1.01
$\tau(B_r)$ (10^{-12} sec)	3.7	7.4	9.5	13.3
$\bar{\tau}(B_r)$ (10^{-12}sec)	2.8	5.3	6.5	...
$n_c(B_r)$ (10^{13} cm^{-3})	6.9	4.3	3.3	2.2

Furthermore, they increase as B increases, at least for photon wavelengths between 337 and 78 μm. This behavior is in contrast to the field-dependent dc mobility time $\tau_0(B)$, whose approximate functional form we have derived from conductivity and Hall data published by Sladek[45] on material similar to but not identical with ours. Figure 4 also illustrates this data for $\tau_0(B)$ (which we estimate to represent our sample to within an error of 50%) and shows that at large fields its

asymptotic behavior is nearly $1/B$, so that $\omega_c\tau_0(B)$ approaches a constant, as suggested by the curve labeled as such. This form agrees with the theory of magnetoresistance for *point* scatterers in the extreme quantum limit as given by Kubo *et al.*[46] but is also characteristic of experimentally determined magnetoconductivities under conditions wherein a variety of scattering mechanisms giving quite different theoretical forms of $\tau(B)$ enter into the problem.[24] Whatever the controlling mechanism, the dc scattering time at 20 kG is about 160 times shorter than the IR time.

The second approach to determining τ took due note of the first and attempted to calculate *a priori* the entire line shape and lengthened scattering times for certain of the lines, using the nonadiabatic and adiabatic times of Eqs. (34) and (35), both of which are increasing functions of B. Because these processes occur simultaneously, the times were added harmonically to obtain a total scattering time $\tau(B, k_z)$. However, both are approximations valid at high fields only, and each yields the
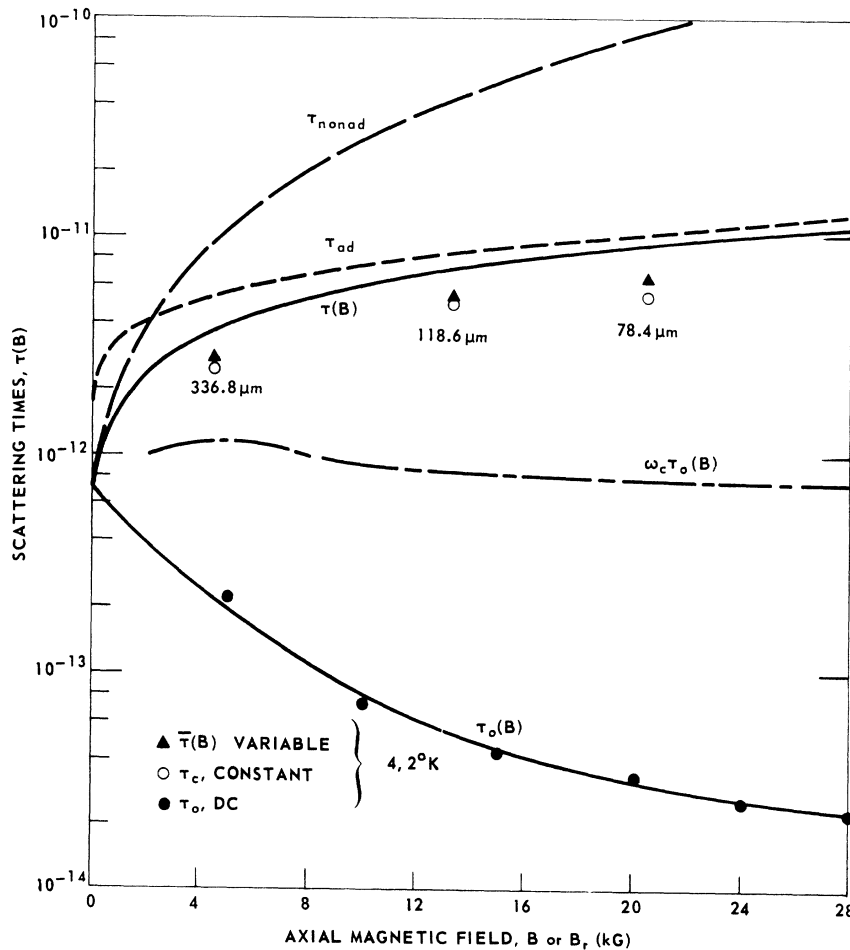

FIG. 4. Scattering times τ vs B. The cyclotron-resonance lines at 337, 119, and 78 μm yield τ_c (open circles) when fitted with constant scattering times. These are much larger than the dc mobility times $\tau_0(B)$, for which $\omega_c\tau_0(B) \approx$ constant. Adiabatic and nonadiabatic Coulomb scattering give τ_{ad}, τ_{nonad}, and $\tau(B)$ as field- and energy-dependent times. Both τ_c and $\bar{\tau}(B_r)$ give essentially the same linewidths, as shown by the triangles and the open circles.

physically nonsensical result $\tau = 0$ at $B = 0$. To cir-
cumvent this, the zero-field dc scattering time
$\tau_0 = 6.8 \times 10^{-13}$ sec was added to $\tau(B, k_z)$ as a means
of obtaining the observed value of τ at $B = 0$. This
adjustment, while unjustified theoretically, is
chiefly a matter of convenience in normalizing the
data of Fig. 4 and may be dispensed with at no loss
to the results. The final expression for the over-
all scattering in this approach is then

$$\tau(B, k_z) = \tau_0 + (\tau_{ad}^{-1} + \tau_{nonad}^{-1})^{-1} . \tag{36}$$

Figure 4 shows the separate contributions from
τ_{nonad} and τ_{ad} (both shifted upwards by τ_0), as well
as the total time $\tau(B, k_z)$ from Eq. (36), with
$k_z = (2mk_BT/\hbar^2)^{1/2}$ evaluated at $T = 4.2\,°K$. Freeze-
out was incorporated into the scattering time by
approximating the carrier-impurity concentration
with a function that matches the experimental data[45]
quite well, namely,

$$N_i(B) = n_c(B) = n_{c0}[1 + B/B_0]^{-1} , \tag{37}$$

where $n_{c0} = 1 \times 10^{14}$ cm^{-3} and $B_0 = 10$ kG. Under these
conditions, τ_{nonad} dominates up to about 2.2 kG,
while τ_{ad} is the controlling time above that. For
the three long-wavelength lines, it may be seen
that not only is the behavior of τ_c as a function of
B predicted satisfactorily by Eqs. (36) and (37),
but the absolute values of τ_c and $\tau(B_r, 4.2°)$ agree
to within a factor of 1.5 to 1.7 as well [compare

the open circles and the line labeled "$\tau(B)$" on
Fig. 4].

The essential correctness of Eq. (36) is further
accentuated when it is used in calculating the actual
cyclotron-resonance line shapes. Figure 3 shows
the computed relative conductivities σ_+/σ_{max} at
$\lambda = 336.8$, 118.6, and 78.4 μm via the dotted lines.
For these three lines we have used the theoretical
values of $\tau(B, k_z)$ in the quantum tensor elements
$\epsilon_\pm(q_z, \omega)$ rather than the experimentally derived
values τ_c (the line at $\lambda = 47.5$ μm used τ_c, however).
Carrier freeze-out is again included by varying
the chemical potential and the absorption param-
eters in concert with n_c. The observed and cal-
culated values of σ_+ at 78.4 and 118.6 μm are in
excellent agreement, while those at 336.8 μm agree
to within 20%. Indeed, the 336.8-μm doublet is
the most difficult one to resolve unambiguously and
the discrepancy quoted is within the experimental
error.

Figure 5 compares calculations of the undistorted
lines at $\lambda = 118.6$ μm which result from the two
approaches. The real part of the normalized con-
ductivity, $\text{Re}(\sigma_+/\sigma_0)$, is plotted using both the theo-
retical values of $\tau(B, k_z)$ and the fitted constant
value $\tau_c = 5.0 \times 10^{-12}$ sec in Eq. (24) (here σ_0 is the
resonant, not the dc conductivity). The curve for
variable collision time tends to be broader in the
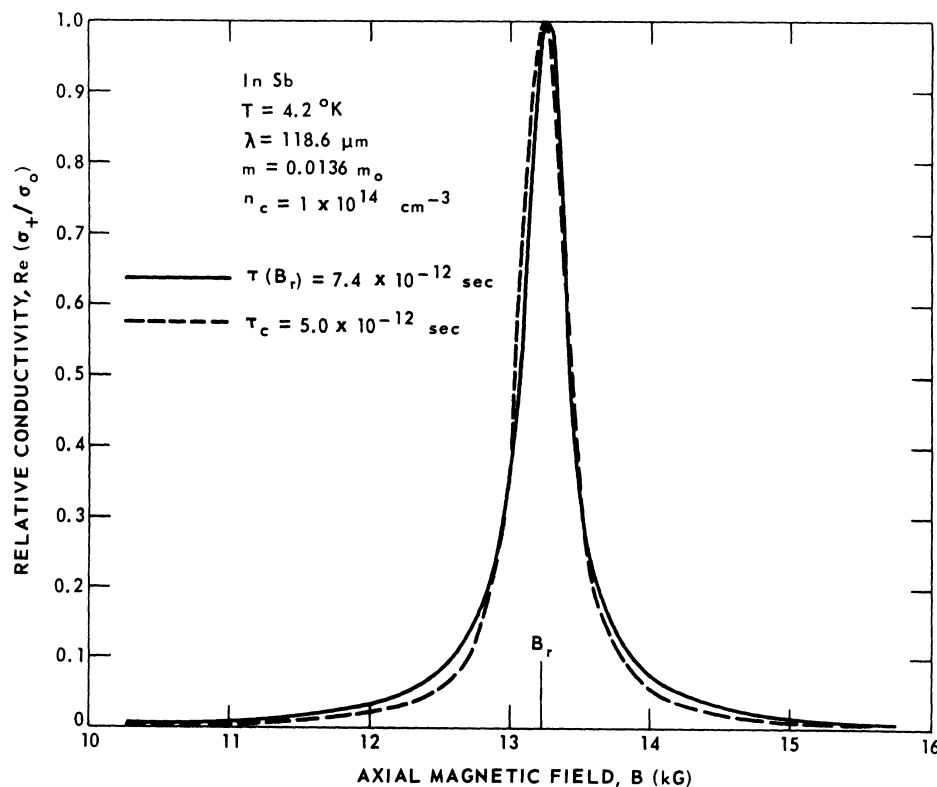wings and more symmetrical, but the differences

In Sb
T = 4.2 °K
λ = 118.6 μm
m = 0.0136 m$_0$
n$_c$ = 1 x 10^{14} cm^{-3}

——— $\tau(B_r)$ = 7.4 x 10^{-12} sec
– – – – τ_c = 5.0 x 10^{-12} sec

FIG. 5. Calculated rela-
tive conductivities at cyclo-
tron resonance showing the
undistorted line shape of a
resonance line at $\lambda = 118.6$
μm. The two profiles re-
sult from the magnetic-field-
dependent scattering $\tau(B, k_z)$
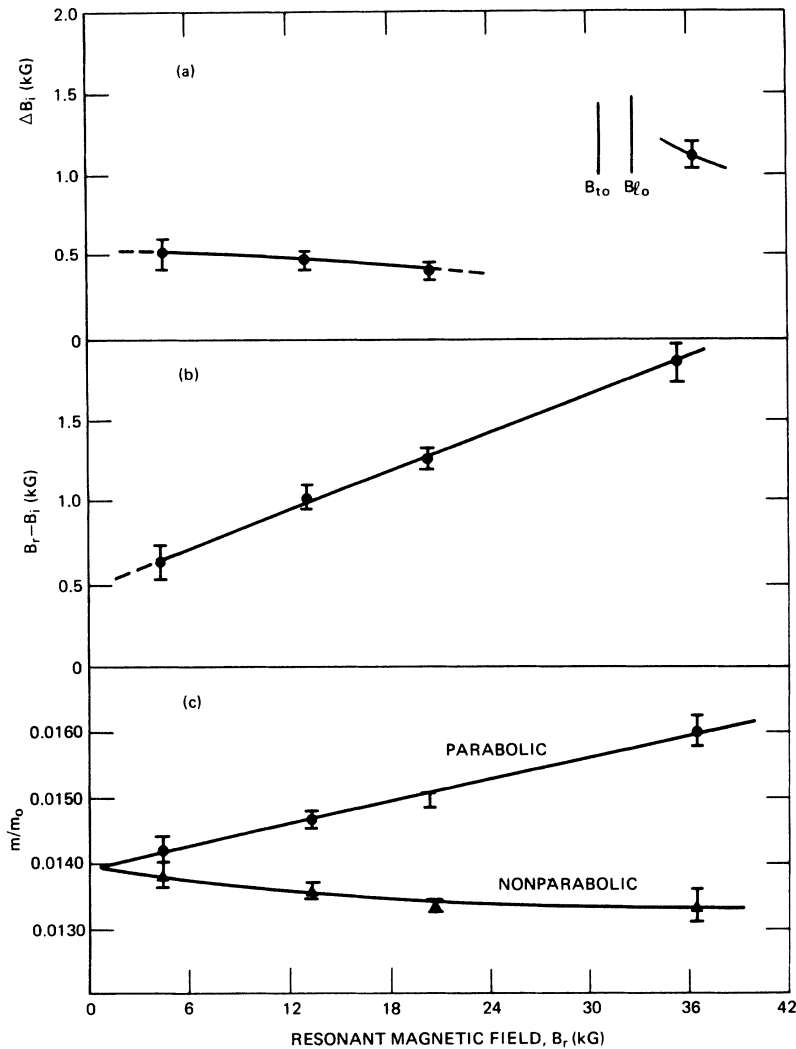and the constant time τ_c.
Both yield approximately the
same half-widths.

FIG. 6. (a) Half-width at half-maximum ΔB_i of the impurity transition. (b) Splitting of cyclotron resonance and impurity doublets. (c) Effective mass from parabolic and nonparabolic levels.

in shapes are on the whole small. Either curve would match the observed conductivities of Fig. 3 to within the experimental error.

From the conductivity curves incorporating $\tau(B, k_z)$, one may define a cyclotron-resonance collision time $\bar{\tau}(B_r)$ by way of the half-widths at half-maximum, $\Delta B_{1/2}$, and resonant field B_r:

$$\bar{\tau}(B_r) = B_r/\omega \Delta B_{1/2} \ . \tag{38}$$

Figure 4 also shows $\bar{\tau}(B_r)$ for the three long-wavelength lines via the solid triangles, which may then be compared directly with τ_c. The agreement is very good, and indeed may be improved by neglecting τ_0 in Eq. (36). Thus, in spite of the somewhat different values of τ_c and $\tau(B, k_z)$ on Fig. 4, the result of integrating the latter over k_z in Eq. (24) to obtain $\bar{\tau}(B_r)$ is a line of essentially the same width but of slightly different shape from that obtained with τ_c. Thus Eq. (36) predicts the field

dependence and absolute values of the observed conductivity widths to within about 10-15% and line shapes to within the experimental error, without the necessity for any adjustable parameters. Such close agreement may be in part fortuitous, of course, but it is nevertheless impressive.

From these results it appears that the line narrowing at high magnetic fields and IR frequencies is due to the decreasing efficacy of long-range ionized impurity scattering in bringing about momentum exchange between electrons and ions. However, the dc mobility suggests that these same processes do not hold at low frequencies, since whatever the exact functional form for $\tau_0(B)$ may be, it is nevertheless a decreasing function of B, while the resonance results yield an increasing $\tau(B)$. One resolution of this contradiction may lie in the frequency dependence of the shielding length $1/k_s$. An ionized impurity that appears shielded for disturbances at $\omega \ll \omega_p$ and which thus presents

a short-range potential to an electron (the Kubo case[42]) will appear to be essentially unshielded for $\omega \gg \omega_p$ (the present regime) and behave as a Coulomb scatterer. Of course, Eq. (36) describes the long-range case. Further investigation of the mechanism is obviously in order.

C. Lattice Interactions

When the energy of an IR photon approaches the lattice-optical-phonon range, the cyclotron-resonance picture changes drastically. Kaplan and Wallis[47] give $\mathcal{E}_{l0} = 24.2$ meV for the longitudinal- and $\mathcal{E}_{t0} = 22.8$ meV for the transverse-optical-phonon energies, which correspond to magnetic fields of $B_{l0} \simeq 32.6$ and $B_{t0} \simeq 30.6$ kG, respectively. The calculated resonant fields at $\lambda = 55.1$ and 47.5 μm straddle these values and both lines are grossly distorted. The 55.1-μm laser line is almost exactly coincident with the transverse optical phonon; the resultant trace has no decipherable form and has not been reproduced here. The attenuation is large but unknown. At 47.5 μm, a very broad resonance occurs that is still interpretable as a doublet, but with most of the electrons apparently immobilized on impurities, so that the free-free transitions are significantly reduced in number.

Several experimental studies[47-50] have shown strong polaron interactions in this region, accompanied by greatly broadened lines. Summers and co-workers,[48] when using material quite similar to ours in terms of n_c and L, observe such effects. They also express suprise at the amount of cyclotron-resonance absorption present. The large absorption, of course, is expained by the present study as arising from the large values of τ, which may have remained unobserved to date because of (a) wide-band sources and (b) apparent distortion due to exponential rather than linear absorption, even in thin samples. At fields above B_{t0}, the theory of Harper[51] satisfactorily explains the broadened lines by way of a coupling of the Landau states with longitudinal optical phonons.

Thus, as regards the data of Fig. 3, the 47.5-μm line is broadened in a two-step process involving photon absorption and then emission of the LO phonon, while the 55.1-μm radiation is probably highly absorbed by direct interaction between photon and TO phonon.

D. Additional Data

Figure 6 illustrates additional information to be derived from the data of Fig. 3. In Fig. 6(a) are shown the impurity line half-widths at half-amplitude, ΔB_i, also exhibiting the discontinuites near the optical-phonon energies. In Fig. 6(b) the solid dots with error flags give the impurity-free electron doublet separation, $B_r - B_i$ in kG, for the four lines in which it was observable.

Figure 6(c) shows the effective-mass ratio vs B for InSb as obtained by fitting the positions of the calculated curves to the experiment. The upper curve marked "parabolic" comes from the simple relation $m/m_0 = eB_r/m_0\omega_c c$ and shows the well-known increase[8] with B in this definition of m; the lower curve labeled "nonparabolic" has utilized Eq. (2) in the dielectric tensor. The mass parameter obtained from the latter is seen to be more nearly constant with increasing B, reflecting the improved $\mathcal{E}(k)$ relation. Both masses extrapolate back to $m/m_0 = 0.0139 \pm 0.0002$, a value which is apparently band model independent; we are suggesting it as the 4.2 °K zero-B mass value in a band filled with electrons at concentration $n_c = 1 \times 10^{14}$ cm^{-3}. This agrees with the band-edge value of 0.0139 ± 0.0001 obtained by Johnson and Dickey.[9]

E. Transmission in Voigt Geometry at 77°K

Using the same sample as above, one resonance measurement was made in the Voigt configuration at 77 °K, whence all the donors are ionized. A line polarizer of about 95% rejection ratio was used and the transmitted signal was detected by an InSb detector mounted in a separate helium Dewar.

Figure 7 shows the free-electron resonance lines at $\lambda = 336.8$ μm with both $\vec{E} \perp \vec{B}$ and $\vec{E} \parallel \vec{B}$, and a theoretical replication of the transverse polarization data using the quantum plasma dielectric element $\epsilon_\perp(\vec{q}, \omega)$ and a constant collision time τ_c. In this geometry, the dispersion relation, Eq. (26), is such that the resonance frequency is shifted to the upper hybrid frequency $(\omega_c^2 + \omega_p^2)^{1/2}$ in the simple model of conductivity. This so-called plasma shift amounts to about 2.2% for the carrier concentration above. If Eqs. (2), (24), and (26) are used, the $0 \rightarrow 1$ transition takes place at a field B_r as marked on the figure.

In the calculation we incorporated spin-up and spin-down transitions having $\Delta n = 1$, $\Delta s = 0$ between the first 20 Landau levels; the last transition contributed less than 1% to the total. Because of the rapidly increasing mass of the higher levels, summing over then gives a line that appears to be shifted toward higher magnetic fields, a fact that could badly mislead one on the effective mass if Eq. (1) were used. The actual 77 °K mass ratio appears to be 0.0132 ± 0.0002. We attribute the shoulder on the high-field side of the line to light holes having a mass $m_{lh} \simeq 0.019 m_0$.[38]

The value of τ_c which gave the excellent fit shown was 2.75×10^{-12} sec, in rough accord with the 77 °K dc time of $\tau_0(B=0) = 5.25 \times 10^{-12}$ sec derived from the static mobility. Since the latter is determined by phonon scattering, the factor-of-2 agreement suggests that the high-frequency conductivity at nitrogen temperature is also controlled by phonons, rather than by impurities, as is the case at 4.2 °K.
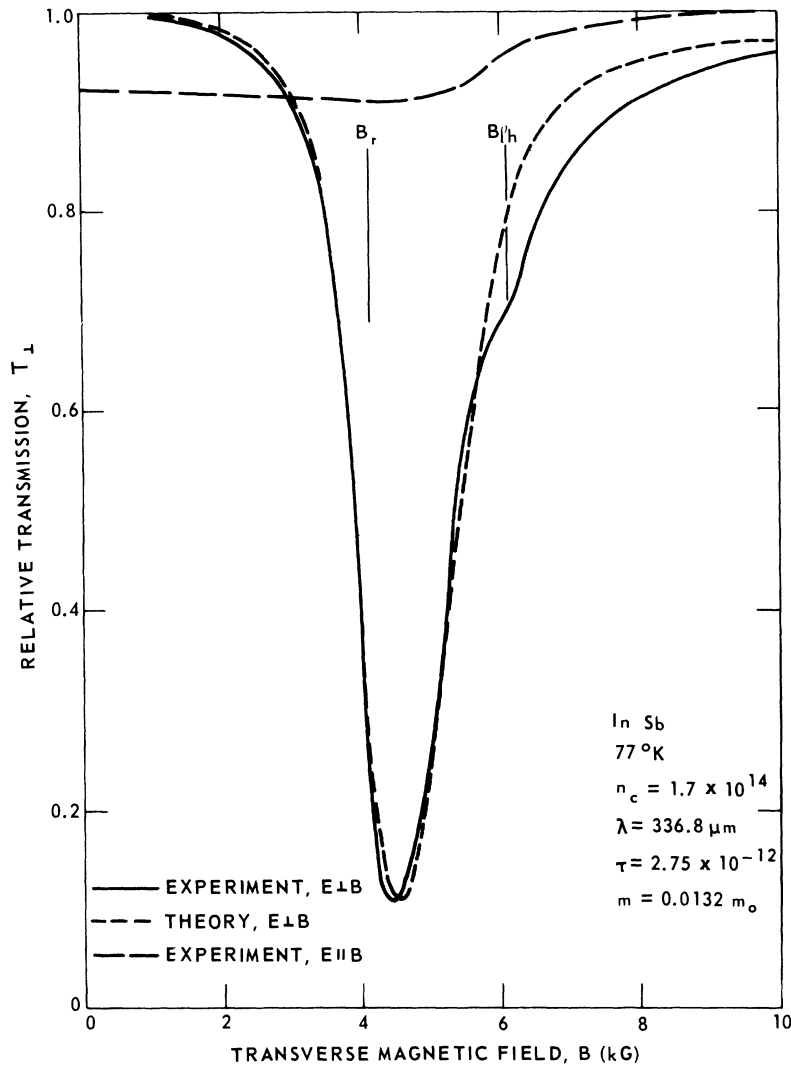
FIG. 7. Cyclotron-resonance line at 77 °K in the Voigt configuration. The 0^+ → 1^+ transition takes place at B_r; 19 higher transitions have been incorporated in the theoretical line shown, which uses a constant scattering time τ_c. Light holes contribute the shoulder shown at B_{lh}.

Both of these scattering times are near the 4.2 °K time of $\tau_c = 2.5 \times 10^{-12}$ sec. Nevertheless, one should not infer a temperature invariance of the IR scattering time from this, since there may exist a maximum in τ at some intermediate temperature, as is the case with the dc mobility. Further variable-T experiments are required in order to illuminate this point.

No use was made of an energy-dependent collision time in the line-shape analysis, since the system is not in the quantum limit at 77 °K and 4.5 kG, and Eq. (36) is not applicable.

When $\vec{E}$ is parallel to $\vec{B}$, a small variation in the transmission is seen which is most likely due to imperfect polarization.

VI. DISCUSSION AND SUMMARY

A satisfactory experimental system for conducting far-IR investigations of solids has been devised

and applied to the study of electron interactions in InSb. The gas laser operates as a source of stable monochromatic signals having wavelengths between 337 and 47 μm; it is possible to extend these wavelengths considerably in both directions. We have shown that cyclotron-resonance measurements with the laser can yield much quantitative information on carrier dynamics when used in conjunction with an adequate theory.

The theoretical formulation chosen is a variant of the quantum plasma dielectric tensor for a free-electron gas and includes energy levels and collision terms appropriate to a real solid. The proper elements of this tensor have been used in the dispersion equation to obtain transmission, absorption, and reflection coefficients that may be compared directly with experiment. These correlations have demonstrated the necessity for the quantum formulation of the plasma dielectric tensor in quantitative work. Measurements of the long-wavelength resonance

line shapes at 4.2 °K imply electron scattering times at IR frequency near 10^{-11} sec, values that are greatly increased over the dc time of 6.8×10^{-13} sec. The dc mobility, however, yields field-dependent times that decrease with B. The experimental transmission coefficients obtained as a function of magnetic field have been compared with calculations made with a sufficiently accurate form of the plasma dielectric tensor, assuming the linewidths to be controlled by long-range ionized impurity scattering. It has been found that adiabatic and nonadiabatic unshielded Coulomb scattering in the quantum limit give the correct widths, shapes, and absorption to within the experimental error. At 77 °K, however, the measured scattering times are within a factor of 2 of the zero-field electron-phonon interaction rates. Thus, Eq. (36) should be applicable to ionized impurity scattering of electrons in the quantum limit, for energies above the plasmon energy but below the optical-phonon region, and at low enough impurity concentrations so that an electron wave packet does not overlap two or more impurity sites.

There are several investigations that await the application of the tools we have outlined. The effect of electron concentration and lattice temperature T upon the Coulomb scattering time should be interesting to observe, the former for its role played in establishing shielding distances and the latter for this, as well as for the generation of phonons. Similarly, energization of electrons above the lattice temperature by the application of an electric field—the hot-electron phenomenon—is particularly well suited for study by way of cyclotron-resonance widths, especially if the scattering time is a reasonably strong function of electron temperature T_e. We are currently investigating several aspects of these effects.

*Present address: NOAA, Atlantic Oceanographic and Meteorological Laboratories, Miami, Fla. 33130.

[1]G. Dresselhaus, A. F. Kip, C. Kittel, and G. Wagoner, Phys. Rev. 98, 556 (1955).

[2]A. Crocker, M. E. Kimmitt, H. A. Gebbie, and L. S. Mathias, Nature 201, 250 (1964).

[3]H. A. Gebbie, N. W. B. Stone, and F. D. Findlay, Nature 202, 685 (1964).

[4]E. Burstein, G. S. Picus, and H. A. Gebbie, Phys. Rev. 103, 825 (1956).

[5]R. J. Keyes, S. Zwerdling, S. Foner, H. H. Kolm, and B. Lax, Phys. Rev. 104, 1804 (1956).

[6]W. S. Boyle and A. D. Brailsford, Phys. Rev. 107, 903 (1957).

[7]B. Lax, J. G. Mavroides, H. J. Zeiger, and R. J. Keyes, Phys. Rev. 122, 31 (1961).

[8]E. D. Palik, G. S. Picus, S. Teitler, and R. F. Wallis, Phys. Rev. 122, 475 (1961).

[9]E. J. Johnson and D. H. Dickey, Phys. Rev. B 1, 2676 (1970).

[10]K. J. Button, H. A. Gebbie, and B. Lax, IEEE J. Quant. Electron. QE-2, 202 (1966).

[11]K. J. Button, B. Lax, and C. C. Bradley, Phys. Rev. Letters 21, 350 (1968).

[12]J. R. Apel, T. O. Poehler, and C. R. Westgate, Appl. Phys. Letters 14, 161 (1969).

[13]R. Kaplan, Appl. Opt. 6, 685 (1967).

[14]R. Turner, A. K. Hochberg, and T. O. Poehler, Appl. Phys. Letters 12, 104 (1968).

[15]R. Turner and T. O. Poehler, Phys. Letters 27, 479 (1968).

[16]R. Turner and T. O. Poehler, J. Appl. Phys. 39, 5726 (1968).

[17]R. Bowers and Y. Yafet, Phys. Rev. 115, 1165 (1959).

[18]Y. Yafet, Phys. Rev. 115, 1172 (1959).

[19]C. R. Pidgeon and R. N. Brown, Phys. Rev. 146, 575 (1966).

[20]R. L. Bell and K. T. Rodgers, Phys. Rev. 152, 746 (1966).

[21]C. R. Pidgeon, D. L. Mitchell, and R. N. Brown, Phys. Rev. 154, 737 (1967).

[22]J. M. Luttinger and W. Kohn, Phys. Rev. 97, 869 (1955).

[23]R. B. Dingle, Proc. Roy. Soc. (London) 211, 500 (1952).

[24]For example, see L. M. Roth and P. N. Argyres, in Semiconductors and Semimetals, Vol. I, edited by R. K. Willardson and A. C. Beer (Academic, New York, 1966).

[25]R. Kaplan, Phys. Rev. 181, 1154 (1969).

[26]R. F. Wallis and H. J. Bowlden, J. Phys. Chem. Solids 7, 78 (1958).

[27]T. H. Stix, The Theory of Plasma Waves (McGraw-Hill, New York, 1962).

[28]M. C. Steele and B. Vural, Wave Interactions in Solid State Plasmas (McGraw-Hill, New York, 1969).

[29]W. R. Allis, S. Buchsbaum, and A. Bers, Waves in Anisotropic Plasmas (MIT, Cambridge, Mass., 1963).

[30]J. R. Apel and T. O. Poehler, The Johns Hopkins University, Applied Physics Laboratory, Technical Memorandum No. TG 1111, 1970 (unpublished).

[31]A. Ron, Phys. Rev. 134, A70 (1964).

[32]A. Kawabata, J. Phys. Soc. Japan 23, 999 (1967).

[33]A. Lodder and S. Fujita, J. Phys. Soc. Japan 25, 774 (1968).

[34]M. P. Greene, H. J. Lee, J. J. Quinn, and S. Rodriguez, Phys. Rev. 177, 1019 (1969).

[35]J. J. Quinn and S. Rodriguez, Phys. Rev. 128, 2487 (1962).

[36]S. D. Smith, in Handbuch der Physik, Vol. XXV/2a, edited by L. Gensel (Springer-Verlag, Berlin, 1967), p. 234.

[37]D. M. S. Bagguley, R. A. Stradling, and J. S. S. Whiting, Proc. Roy. Soc. (London) 262, 340 (1961).

[38]D. M. S. Bagguley, M. L. A. Robinson, and R. A.

Stradling, Phys. Letters 6, 143 (1963).

[39]J. M. Chamberlain and R. A. Stradling, Solid State Commun. 7, 1275 (1969).

[40]A. L. Mears and R. A. Stradling, Solid State Commun. 7, 1267 (1969).

[41]J. R. Apel, T. O. Poehler, and C. R. Westgate, Solid State Commun. 8, 1693 (1970).

[42]R. Kubo, S. J. Miyake, and H. Hashitsume, in *Solid State Physics*, Vol. 17, edited by F. Seitz and D. Turnbull (Academic, New York, 1965), p. 269.

[43]H. Kawamura, H. Saji, M. Fukai, K. Sekido, and I. Imai, J. Phys. Soc. Japan 19, 288 (1964).

[44]S. J. Miyake, J. Phys. Soc. Japan 20, 412 (1965).

[45]R. J. Sladek, J. Phys. Chem. Solids 5, 157 (1958); 8, 515 (1959).

[46]Reference 42, p. 255.

[47]R. Kaplan and R. F. Wallis, Phys. Rev. Letters 20, 1499 (1968).

[48]C. J. Summers, R. B. Dennis, B. S. Wherrett, P. G. Harper, and S. D. Smith, Phys. Rev. 170, 755 (1968).

[49]B. D. McCombe and R. Kaplan, Phys. Rev. Letters 21, 756 (1968).

[50]R. C. Enck, A. S. Saleh, and H. Y. Fan, Phys. Rev. 182, 790 (1969).

[51]P. G. Harper, Proc. Phys. Soc. (London) 92, 793 (1967).

Electronic Core Levels of the IIB-VIA Compounds

C. J. Vesely* and D. W. Langer

Aerospace Research Laboratories, Wright-Patterson Air Force Base, Ohio 45433

(Received 22 March 1971)

X-ray induced electron-emission measurements were used to determine the energy levels of core electrons in ZnO, ZnS, ZnSe, ZnTe, CdO, CdS, CdSe, CdTe, HgS, HgSe, and HgTe. The investigated energy range extends from the bottom of the valence band to about 1200 eV below the Fermi level. Chemical shifts were determined by comparing our results with experimental values for the pure elements. These shifts are plotted as a function of the fractional ionicity values determined by Phillips and Van Vechten, Pauling, and Coulson. Spin-orbit-splitting values were experimentally determined for the first time for several levels including the $Zn 3d$, $Cd 4d$, and $Hg 5d$ levels. Furthermore, our measured energy values for these levels are used to determine the absolute energy values of the initial and final states of transitions normally labeled d_2 in ultraviolet reflectivity and electron-energy-loss measurements. Our results for ZnSe and CdTe are compared with self-consistent relativistic orthogonalized-plane-wave calculations for the excitation energies of these compounds. Agreement with these theoretical calculations is best for the levels closest to the valence band and appears to be angular momentum dependent.

I. INTRODUCTION

The purpose of this paper is to present the results of our x-ray induced electron-emission studies of ZnO, ZnS, ZnSe, ZnTe, CdO, CdS, CdSe, CdTe, HgS, HgSe, and HgTe. The merits of this experimental technique with respect to other procedures such as x-ray absorption and emission, ultraviolet (uv) reflection and absorption, and electron-energy-loss measurements have already been discussed.[1-3]

Section II consists of a description of the experimental procedure. It includes a brief description of the equipment used to make the measurements and a more detailed discussion of the principles of operation as applied to the measurement of semiconductors. This includes a description of the procedures we followed in order to correct for the amount of charge buildup on the samples.

We discuss the results of our measurements in Sec. III which we have divided into four parts. The first part is concerned with the actual location of the energy levels. We list our results and compare them with published experimental data for the pure elements. Our results for ZnSe and CdTe are also compared with theory. In the second part we compare the spin-orbit-splitting values we measured

with experimental values for the pure elements and with theoretical values for the elements in the form
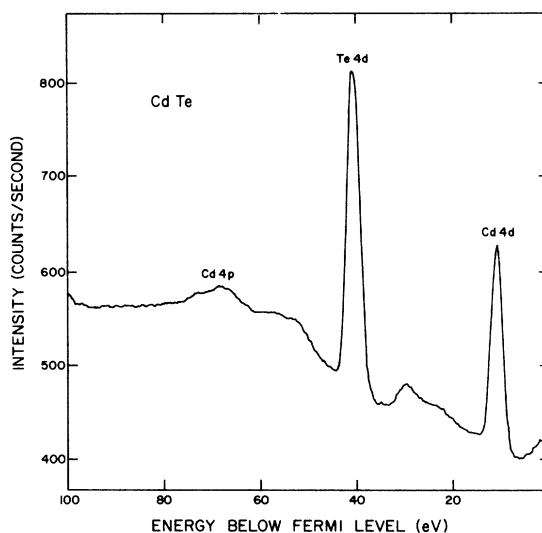

FIG. 1. Electron-emission spectrum of CdTe. The range of binding energies extends from the Fermi level to 100 eV below the Fermi level.